

Design and Analysis of an Innovative Dead-end Cascade-type PEMFC Stack at Different Orientations

M. Rahimi-Esbo^{a,*}, M. M. Barzegari^a, M. Khorshidian^b, S. M. Rahgoshay^{c,*}

^a Assistant professor, North Institute of Science & Technology, Malek Ashtar University of Technology, Iran.

^b Researcher, North Institute of Science & Technology, Malek Ashtar University of Technology, Malek Ashtar University of Technology, Iran.

^c Researcher, North Institute of Science & Technology, Malek Ashtar University of Technology, Malek Ashtar University of Technology, Iran.

Article Information

Article History:

Received:

12 October 2020

Received in revised form:

9 November 2020

Accepted:

15 November 2020

Keywords

Experimental study
Cascade-type PEM fuel cell
Dead-end condition
Stack design

Abstract

In this paper, the design and experimental study of a 4-cells cascade-type H_2/O_2 polymer electrolyte membrane (PEM) fuel cell stack with integrated humidifiers and water separators are presented. The PEM fuel cell stack is subdivided into two stages to minimize the quantity of exhaust gases during operation. A dead-end condition is applied for both cathode and anode sides of the PEM fuel cell stack. In a dead-end mode, the end-stage is designed to entirely use the reactant gases in the operation. Periodical purging is utilized to remove the accumulated water or impurities from the cascade-type PEM fuel cell stack. Comparison of cascade-type PEM fuel cell stack operation in a dead-end mode with a flow-through mode is performed. Results revealed that integrating humidifiers and water separators with the stack improved the volume power density of the PEM fuel cell stack. Moreover, since more liquid water was produced on the cathode side, the fluctuation of purge cell voltage of the cathode side is higher than that of the anode side. In addition, a technique is applied to control the pressure fluctuation of both sides of the PEM fuel cell.

*Corresponding author: mrahimi@mut.ac.ir

Corresponding author: rahgoshay@mut.ac.ir

majid.rahgoshay@gmail.com

Nomenclature

				n_d	electro-osmotic drag coefficient	ϵ	gas diffusion layer porosity
an	anode	R_m	equivalent membrane resistance to proton conduction(Ω)	p	pressure(Pa)	θ_c	contact angle (.)
atm	atmosphere	R_{ohmic}	internal electrical resistance	p_c	capillary pressure (Pa)	λ	membrane water content
A	area(m ²)	R_{O_2}	oxygen gas constant (J(kgK) ⁻¹)	p_{sat}	saturation pressure (Pa)	μ_l	viscosity of water (kg(ms) ⁻¹)
ca	cathode	R_v	vapor gas constant (J(kgK) ⁻¹)	p	power (w)	$\rho_{memb,dry}$	membrane dry density
D_v	diffusion coefficient(m ² s ⁻¹)	s	liquid water saturation	PID	proportional integral derivative	ρ_w	water density
D_w	membrane vapor transfer coefficient (m ² s ⁻¹)	S_{im}	immobile saturation	PT	pressure transmitter	σ	surface tension
eff	effective	S	reduced liquid water saturation	R	universal gas constant (J(k-gK) ⁻¹)	ϕ	relative humidity
evap	evaporation	S_i	i th section of fuel cell	R_c	equivalent contact resistance to electron conduction		
E_{Nernst}	thermodynamic potential (V)	st	stack	R_{H_2}	hydrogen gas constant		
FC	fuel cell	st_i	i th stage of fuel cell				
F	Faraday's constant	t	Time (s)				
FT	flow transmitter	t_{GDL}	gas diffusion layer thickness(m)				
Hu	humidifier	t_m	membrane thickness (m)				
i_{FC}	current density(Acm ⁻²)	t_p	purge time (s)				
I_{st}	stack current (A)	T	temperature (k)				
k	orifice constant (kg(sPa) ⁻¹)	TT	Temperature transmitter				
K	absolute permeability (m ²)	v	vapor				
l	liquid	V	volume (m ³)				
LC	level controller	VC	voltage controller				
m	mass (kg)	V_{act}	activation loss (v)				
memb	membrane	V_{conc}	concentration loss (v)				
M_{H_2}	hydrogen molar mass (kgmol ⁻¹)	V_{ohmic}	ohmic loss (v)				
$M_{memb,dry}$	membrane dry equivalent weight (kg-mol ⁻¹)	V_p	volume of gas diffusion layer porosity (m ³)				
M_{O_2}	oxygen molar mass (kgmol ⁻¹)	V_{st}	stack voltage (v)				
M_v	vapor molar mass (kgmol ⁻¹)	a_i	flooding coefficient				
n	number of cells	γ	volumetric condensation coefficient (s ⁻¹)				

1.Introduction

Fuel cells are devices that convert fuel and oxidant directly into electrical energy and can be used in a wide diversity of applications. Wilberforce et al. [1] produced an overview of fuel cell technology and its advantages and disadvantages as compared with competitive technologies. Moreover, they studied the main features and applications of different fuel cell types in stationary and portable sectors.

In recent years, the proton exchange membrane fuel cell (PEMFC) has been considered as an alternative for both stationary and mobile applications due to its high energy conversion efficiency, high power density, quick startup, and low environmental pollution [2-5]. The PEMFC's operation mode can be classified into the flow-through mode, recirculation mode, and dead-end mode [6]. In a flow-through mode, the reactant gases have to be supplied in excess to remove the accumulated water by the convective force of the excess gas flow. In a recirculation mode, the unused reactant gases are returned to the inlet by a pump or compressor. In a dead-end mode, the reactant gases are supplied at the exact rate at which they are being consumed.

Accumulation of liquid water at both the anode and cathode sides of a PEM fuel cell causes water flooding, which reduces the catalytic active sites [7, 8]. Water flooding can block mass transfer and result in fuel starvation, carbon corrosion, and catalyst degradation [9]. In a customary PEMFC stack made up of a single-stage cathode and anode, the reactant gases are supplied in excess (at a stoichiometric ratio much higher than 1) to prevent water flooding of the gas diffusion layers (GDLs) [10]. However, in the dead-end mode, there is a high risk of fuel starvation, which results in unstable stack voltages and membrane electrode assembly (MEA) degradation [11]. The anodic dead-end mode PEM fuel cell has been studied by several researchers, but there have been only a few investigations of the cathodic dead-end mode PEMFC [12, 13].

Reactant utilization is the mass flow rate of reactants at either the cathode or the anode side of the PEMFC that is consumed in the cell divided by the inlet mass flow rate of oxygen or hydrogen, respectively. Several studies have been performed to improve reactant utilization. Nishikawa et al. [14] suggested a strategy for high fuel utilization based on stack separation methods using humidification cells inside the cathode that can operate at high efficiency without the need for supplementary power. They demonstrated a fuel utilization of 96% for a 5 kW-class PEM fuel cell stack. Uno et al. [15] proposed a pressure swing recirculation system that operated using two check valves and fluid control devices without any recirculation pumps. They studied the performance of the proposed system for a single fuel cell. Lee et al. [16] experimentally studied the characteristics of water transport through the membrane for different values of operating parameters, such as the relative humidity, stoichiometry of air, current density, location of humidification, and membrane thickness. They applied a dead-end mode in the PEMFC system to evaluate the water-transport characteristics by observing the performance degradation of the PEMFC and by visualizing the accumulation of water. Hou et al. [17] experimentally investigated the dynamic characteristics of actual hydrogen consumption under the step load variation and hydrogen purge operation of a PEMFC. They improved the

dynamic model of hydrogen consumption by considering the effects of a hydrogen purge operation. They validated the model with experimental data under three different operating conditions.

Chen et al. [18] investigated an anode purge strategy of a single cell based on nitrogen accumulation. They reported that cycle duration decreased with increasing current density during the anodic dead-end mode operation of a single cell. Belvedere et al. [19] investigated the water flooding phenomenon of a PEM fuel cell according to performance degradation. They reported that an optimized purge process increases the fuel utilization factor. Hwang et al. [20] experimentally investigated the effects of different hydrogen supply schemes on the efficiency of a PEMFC system. They used smart control strategies to study the performance of a fuel cell in both the dead-end mode and the recirculation mode.

Since water flooding can affect the PEM fuel cell performance and durability, a cascade-type stack design is employed to resolve these problems and to minimize the exhaust gases from the stack. A fuel cell system of this type is usually fed by pure hydrogen and pure oxygen. Han et al. [13] developed a cascade-type PEM fuel cell stack for an underwater vehicle. The proposed cascade-type stack exhibited high hydrogen and oxygen utilization of 99.89% and 99.68%, respectively, and resulted in notably less purge-gas emissions outside the stack. Cascaded fuel cells include several stages, each having at least one fuel cell block, operating gas feed, and operating gas discharge. The end-stage of a cascaded fuel cell has an operating gas feed connected to the operating gas discharge of the preceding stage. In the dead-end mode, the end-stage is designed in such a way that it entirely uses the reactants in its operation (Stoichiometry~1) [6]. Barzegari et al. [21] presented a nonlinear model of a cascade-type stack composed of two stages. Ordinarily, periodical purging is used to remove the produced water of a dead-ended stack. Han et al. [22] designed and tested a 15 kW-class PEMFC stack to study the effectiveness of their proposed design. The experimental results showed that the amount of purge gas was significantly decreased, and fuel utilization of more than 99.6% was achieved. Bizon [23] proposed

a new strategy based on a real-time switching of fueling regulators' inputs for better fuel saving in PEMFC systems. It was reported that the fuel consumption was reduced compared to commercial strategies. Chen et al. [24] investigated performance degradation and recovery characteristics during the purging process in a PEM fuel cell at the dead-ended anode mode under different operating conditions. They concluded that performance recovery time can be reduced by increasing the current density, cathode relative humidity, and operating temperature. Ge et al. [25] developed an alternating current impedance-based method to identify cathode corrosion in a PEM fuel cell operating in the dead-end anode mode. They reported that voltage change in the anode is exclusively due to sudden rises in the cathode polarization resistance. Dashti et al. [26] developed a mathematical model by incorporating nitrogen crossover from the cathode to the anode and water accumulation in the anode of a dead-end anode PEMFC. They suggested that purge parameters can be optimized by using this model and proposed the concept of 'total wasted energy'. Steinberger et al. [27] introduced and experimentally investigated two purge strategies that enable fuel cell operation with up to 30 vol.% nitrogen content in the fuel gas. They reported that the discontinuous purge strategy is less efficient than the continuous type up to a level of 98% volume fraction hydrogen content in the fuel gas.

Because the water separators are arranged between the stages, the produced water of each stage is separated from the gas and not flushed into the following stage, which prevents the PEMFCs from being flooded by water [28]. Maintaining proper membrane humidity is also very important to guarantee the optimal operation of a PEM fuel cell system, so oxygen and hydrogen humidifiers are utilized to humidify the dry reactants [29]. Using an integrated humidifier and water separator decreases the occupied space and increases the modularity of the system. In addition, it reduces the number of leaking points in the PEMFC stack; thereby, decreasing the needed supply of reactant gases, particularly important in fuel cell systems used in aerospace applications.

In this work, a 4-cells dead-end cascade H_2/O_2 PEM fuel cell stack with integrated humidifiers and water

separators was designed, fabricated, and tested. Humidifiers and water separators were integrated with the stack. The PEM fuel cell stack was subdivided into two stages to minimize the quantity of exhaust gases during operation. Both anode and cathode sides of the PEMFC stack operated in the dead-end mode. Periodical purging was utilized to remove accumulated water or impurities from the cascade-type PEM fuel cell stack. ; of the cascade-type PEM fuel cell stack performance in a dead-end mode with a flow-through mode was carried out.

2.New stack design

Fig. 1 shows a schematic figure of the proposed design of a cascade-type PEM fuel cell stack with integrated humidifiers and water separators. The cascade region has two stages; the first stage has three cells and the second one has one cell. As can be seen, the anode and cathode sides of the PEM fuel cell are fueled by hydrogen and oxygen, respectively. Proper humidity of reactants is ensured by using the humidifiers to minimize the danger of membrane dehydration. The number of humidifier cells is considered to be two that each of cells humidifies a dry reactant. Moreover, water separators are utilized between the first and the second stages for both cathode and anode sides of the PEMFC stack to remove the accumulated water from the gas. The PEMFC stack characteristics are presented in Table 1.

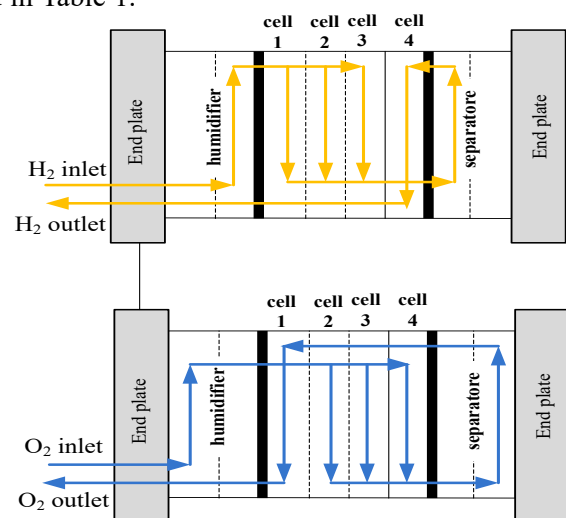


Fig. 1. Schematic illustration of a dead-end cascade H_2/O_2 PEM fuel cell stack with integrated humidifiers and water separators.

Table 1. PEMFC Stack Characteristics.

Parameter	Active area	Stack dimension (width×height×length)	Number of cells	Pressure clamp
Value	225 cm ²	30 cm×40 cm×25 cm	4	6 N.m

3. PEM fuel cell test bench

The experimental data were obtained from a 400W PEMFC stack consisting of 4 cells with a 225 cm² membrane manufactured by PaxiTech. The fabricated cascade-type PEM fuel cell stack is depicted in Fig. 2.

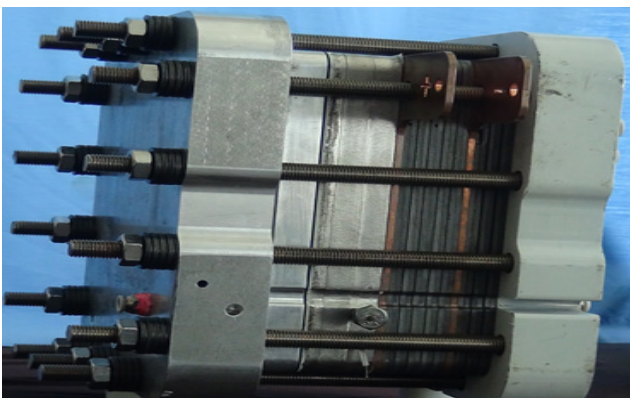
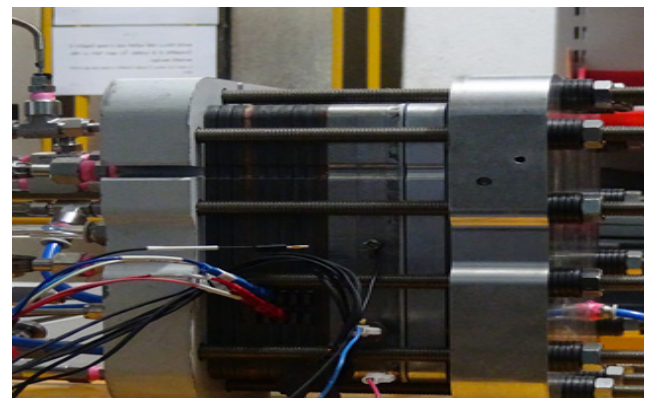


Fig. 2 A 4-cells dead-end cascade H₂/O₂ PEM fuel cell stack with integrated humidifiers and water separators.

The PEMFC stack utilized a water-cooling system due to its better power density compared to air-cooled fuel cell stacks. Two humidifier cells are considered for the system to humidify the two dry reactants. Moreover, it is assumed that there are water separators between the first and second stages for both cathode and anode sides of the PEMFC stack.



The experimental PEM fuel cell stack on a test bench is shown in Fig. 3. The energy produced by the PEMFC stack is delivered to a 5 kW electronic load. The operator communicates with the test bench through a graphic LabVIEW2018 interface that was constructed for the control and monitoring of the PEMFC stack. The individual cell voltages can be measured using voltage monitoring cables.

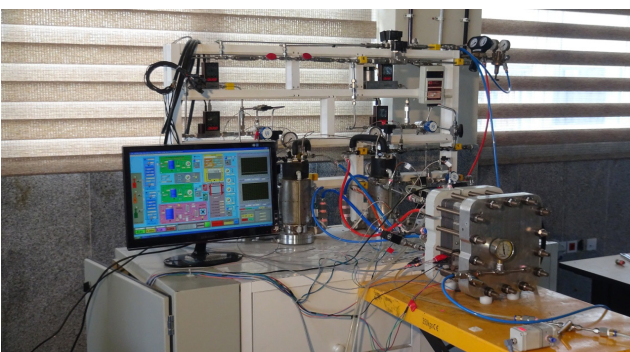


Fig. 3 The PEM fuel cell bench setup.

The process flow diagram (PFD) of the test bench is presented in Fig. 4. Hydrogen and oxygen were fed into the integrated planner humidifiers and water separators before entering the stack. The inlet pressure of reactant gases was controlled using forward pressure regulators. The unconsumed gases were intermittently discharged into the surrounding environment by opening the purge valves. The purge gas flow rates were measured using mass flow indicators installed at the anode and cathode outlets of the stack. The inlet and outlet temperatures of the cooling water were regulated by a PID controller, which set the fan speed and changed the heat transfer rate of the radiator.

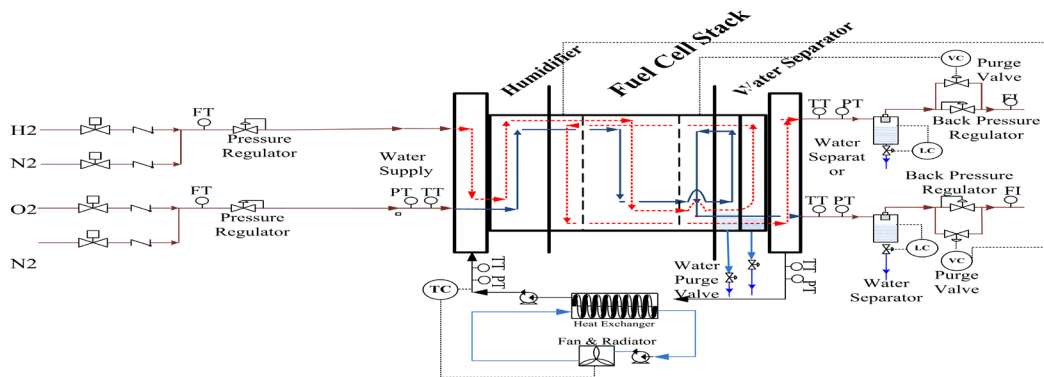


Fig. 4 Process flow diagram of the applied test bench.

4. Mathematical modeling

This paper presents a zero-dimensional model composed of two main modules: a fluid dynamics model (hydrogen, oxygen, liquid water, and vapor) and an electrochemical static model. The dynamic mathematical model includes mass balances for the oxygen and hydrogen humidifiers, mass balances for the anode and cathode side of the PEMFC stack, equations for the membrane, and electrochemical equations. Based on the position of the anode and cathode stages, the fuel cell stack is subdivided into three sections [3].

4.1. Humidifier mathematical model

In this section, mathematical models of the humidifiers are studied. Pure dry oxygen and hydrogen were used as the oxidant and fuel, respectively, which are supplied to the oxygen and hydrogen humidifiers. The oxygen humidifier model describes the humidity of the oxygen entering the 1st stage of the PEMFC stack's cathode side. The equations are based on mass continuity to balance the mass of the components as follows [3]:

$$\dot{m}_{o_2, Hu(o_2)} = \dot{m}_{o_2, in, Hu(o_2)} - \dot{m}_{o_2, out, Hu(o_2)} \quad (1)$$

$$\dot{m}_{v, Hu(o_2)} = \dot{m}_{v, memb, Hu(o_2)} - \dot{m}_{v, out, Hu(o_2)} \quad (2)$$

where $\dot{m}_{v, memb}$ is the water mass flow rate across the membrane.

The hydrogen humidifier model is similar to the oxygen humidifier model. As shown in Fig. 1, the humidified hydrogen enters the 1st stage of the stack's anode side. The mass balance equations of the hydrogen humidifier can be defined as follows [3]:

$$\dot{m}_{H_2, Hu(H_2)} = \dot{m}_{H_2, in, Hu(H_2)} - \dot{m}_{H_2, out, Hu(H_2)} \quad (3)$$

$$\dot{m}_{v, Hu(H_2)} = \dot{m}_{v, memb, Hu(H_2)} - \dot{m}_{v, out, Hu(H_2)} \quad (4)$$

The subscript "Hu(o₂)" and "Hu(H₂)" refer to the oxygen and hydrogen humidifiers, respectively.

4.2. Water separators mathematical model

As demonstrated in Fig. 1, water separators that completely remove the liquid water of the cathode and the anode before entering the next stage are arranged between the two stages of the PEMFC stack. These water separators prevent the stack from water flooding. According to the assumption, $\dot{m}_{l, an, in, FC(S_i)}$ and $\dot{m}_{l, ca, in, FC(S_i)}$ should be zero. The subscript "FC(S_i)", "an" and "ca" express the *i*th section, the anode side, and the cathode side of the stack, respectively.

4.3. Cascade-type PEMFC stack mathematical model

In this section, the mathematical model of a cascade-type PEM fuel cell stack is provided. The mass balance equations of the anode side of the 1st, 2nd, and 3rd sections can be presented in the following form [3]:

$$\dot{m}_{H_2,FC(S_i)} = \dot{m}_{H_2,in,FC(S_i)} - \dot{m}_{H_2,out,FC(S_i)} - \dot{m}_{H_2,reacted,FC(S_i)} \quad (5)$$

(6)

$$\dot{m}_{v,an,FC(S_i)} = \dot{m}_{v,an,in,FC(S_i)} - \dot{m}_{v,an,out,FC(S_i)} - \dot{m}_{H_2,an,GDL2ch,FC(S_i)} + \dot{m}_{evap,an,FC(S_i)} \quad (7)$$

$$\dot{m}_{l,an,FC(S_i)} = -\dot{m}_{l,an,GDL2ch,FC(S_i)} - \dot{m}_{l,an,out,FC(S_i)} - \dot{m}_{evap,an,FC(S_i)}$$

Moreover, the mass balance equation of the cathode side of the 1st, 2nd and 3rd sections of the PEMFC can be defined as follows [3]:

(8)

$$\dot{m}_{O_2,FC(S_i)} = \dot{m}_{O_2,in,FC(S_i)} - \dot{m}_{O_2,out,FC(S_i)} - \dot{m}_{O_2,reacted,FC(S_i)} \quad (9)$$

$$\dot{m}_{v,ca,FC(S_i)} = \dot{m}_{v,ca,in,FC(S_i)} - \dot{m}_{v,ca,out,FC(S_i)} + \dot{m}_{v,ca,GDL2ch,FC(S_i)} + \dot{m}_{evap,ca,FC(S_i)} \quad (10)$$

$$\dot{m}_{l,ca,FC(S_i)} = \dot{m}_{l,ca,GDL2ch,FC(S_i)} - \dot{m}_{l,ca,out,FC(S_i)} - \dot{m}_{evap,ca,FC(S_i)}$$

where $i=1,2,3$ and $\dot{m}_{H_2,reacted}$, $\dot{m}_{O_2,reacted}$ and \dot{m}_{evap} denote reacted hydrogen, reacted oxygen, and evaporation mass flow rates, respectively. Moreover, $\dot{m}_{v,GDL2ch}$ and $\dot{m}_{l,GDL2ch}$ express the mass flow rates of vapor and liquid from the gas diffusion layer to the channel, respectively.

Water steam partial pressures inside the anode and the cathode gas diffusion layer are evaluated as [3]:

$$\text{with } i=1,2,3 \quad (11)$$

$$\dot{P}_{v,an,GDL,FC(S_i)} = RT_{FC} \left(\frac{N_{v,an,FC(S_i)} - N_{v,memb,FC(S_i)}}{t_{GDL}} + R_{evap,an,FC(S_i)} \right)$$

$$\text{with } i=1,2,3 \quad (12)$$

$$\dot{P}_{v,ca,GDL,FC(S_i)} = RT_{FC} \left(\frac{N_{v,gen,FC(S_i)} - N_{v,memb,FC(S_i)} - N_{v,ca,FC(S_i)}}{t_{GDL}} + R_{evap,ca,FC(S_i)} \right)$$

R is the ideal gas constant and t_{GDL} is the GDL thickness. The liquid water volume of both the anode and the cathode sides is derived based on mass balances as [3]:

$$\text{with } i=1,2,3 \quad (13)$$

$$\rho_w V_{l,an,GDL,FC(S_i)} = m_{l,an,GDL2ch,FC(S_i)} - R_{evap,an,FC(S_i)} M_v \varepsilon V_{GDL}$$

$$\text{with } i=1,2,3 \quad (14)$$

$$\rho_w V_{l,ca,GDL,FC(S_i)} = m_{l,ca,GDL2ch,FC(S_i)} - R_{evap,ca,FC(S_i)} M_v \varepsilon V_{GDL}$$

Where M_v is the molar mass of vapor, ρ_w is the water density, and ε is the GDL porosity. Moreover, V_p is the volume of GDL porosity.

4.4. PEMFC stack electrochemical model

The voltage of a single fuel cell depends on the open circuit voltage of the fuel cell (E_{Nernst}), the activation loss (V_{act}), the ohmic loss (V_{ohmic}), and the concentration loss (V_{conc}). Moreover, the stack voltage (V_{st}) can be obtained as the sum of the individual cell voltages [10]:

(15)

$$V_{st} = \sum_{i=1}^3 V_{FC(S_i)} = \sum_{i=1}^3 n_{s_i} (E_{Nernst,FC(S_i)} - V_{act,FC(S_i)} - V_{ohmic,FC(S_i)} - V_{conc,FC(S_i)})$$

The definition of different parameters is described in the appendix.

5. Result and discussion

Before studying the performance of the 4-cells cascade-type PEMFC, the stack is conditioned for almost three hours according to the PaxiTech Company conditioning procedure. The variation of voltage and current density is depicted in Fig. 5. During the break-in process, the variation of current density at a constant voltage is recorded. As shown in Fig. 5, the current density has no considerable change after three hours, which means that the break-in process is complete.

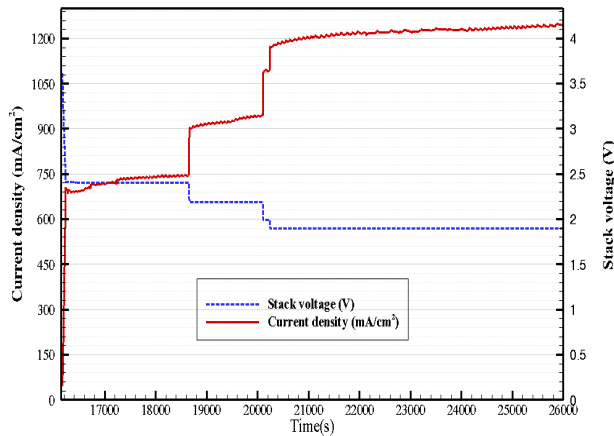


Fig. 5 Stack voltage and current density in the break-in process (inlet humidity of reactants~100%, stoichiometry ($H_2=1.2$ and $O_2=1.5$), temperature=80°C, inlet pressure of reactants= 2 bar g).

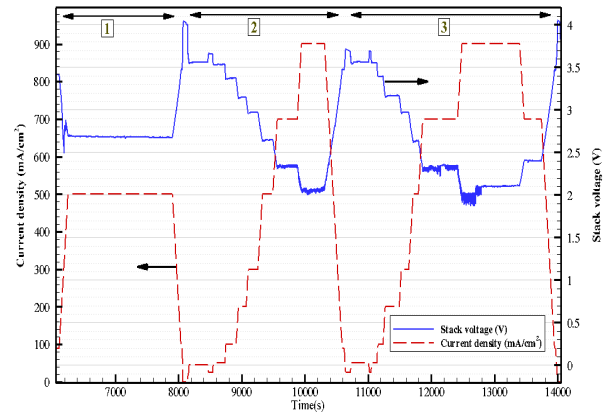


Fig. 6: Variation of voltage and current density with respect to time. (1) Pre-conditioning, (2) Polarization curve measurement in the flow-through mode, and (3) Polarization curve measurement in the dead-end mode.

After pre-conditioning the MEAs, the PEM fuel cell stack is tested for extracting a polarization curve. Fig. 6 demonstrates the variations of voltage and current density with respect to time, including (1) pre-conditioning, (2) polarization curve measurement in the flow-through mode, and (3) polarization curve measurement in the dead-end mode. While extracting the polarization curve, 10 steps were considered to change the current from an open circuit voltage mode to the maximum current density. In each step, the steady amount of voltage was recorded.

The results (polarization curve) of the dead-end mode are compared with the flow-through mode in Fig. 7. As can be seen, the performance of the cascade-type PEMFC stack operating in the dead-end mode is the same as the performance in the flow-through mode. However, according to the low purge flow rate of hydrogen (less than 0.3%), the efficiency of the dead-end mode is higher than the flow-through mode. The details of the test conditions are listed in Table 2. It should be noted that the 1st and 4th cells of the PEMFC stack were considered to be purge cells (Fig. 1). The 1st cell was considered the purge cell for oxygen, and the 4th cell was considered the purge cell for hydrogen. By varying the oxygen and hydrogen purge cells, no specific cell will be in a state of fuel and oxidant starvation.

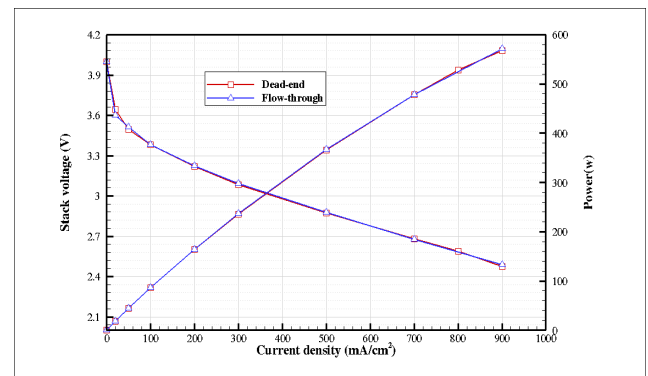


Fig. 7: Polarization curves of the dead-end and flow-through cascade H_2/O_2 PEMFC stack.

Fig. 8 exhibits the polarization curve of the PEM fuel cell for three different configurations, including a conventional stack (stack with an external separator and humidifier operating in the flow through mode), a stack with integrated humidifiers, and a stack with integrated humidifiers and water separators. As shown, integrating humidifiers and water separators resulted in a considerable improvement in PEM fuel cell performance, i.e., an increase in relative humidity of reactants at the stack inlet, uniform temperature distribution, and omitting the external piping component. Moreover, the power density of the stack with integrated humidifiers and water separators increased due to the extreme reduction of stack volume.

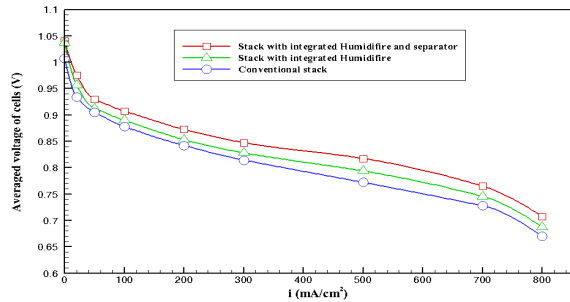


Fig. 8 Polarization curves of a dead-end cascade PEMFC stack for three different PEMFC designs.

Table 2. Test Conditions.

Inlet humidity of reactants (%)	Stoichiometry of H ₂ & O ₂ (flow-through mode)	Stoichiometry of H ₂ & O ₂ (dead-end mode)	Inlet pressure of reactants (bar g)	Temperature (°C)
≈100	1.2 & 1.5	1.003 & 1.01	1	70

The effect of stack orientation on the performance of the PEM fuel cell is illustrated in Fig. 9. In this figure, changes in stack voltage and stack power with respect to current density are displayed under three different orientations (-35°, 0°, and +35°). This test was carried out to study the performances of the water separators and stack under various orientations. Increasing the cell orientation results in an increase in gradient force along the flow direction; therefore, the removal of produced water improves. This is the main reason for the performance improvement at the orientation angle of +35°. On the contrary, at the orientation angle of -35°, the gradient force acts along the reverse direction of water droplet flow. Hence, the performance of the stack decreases due to the water flooding phenomenon.

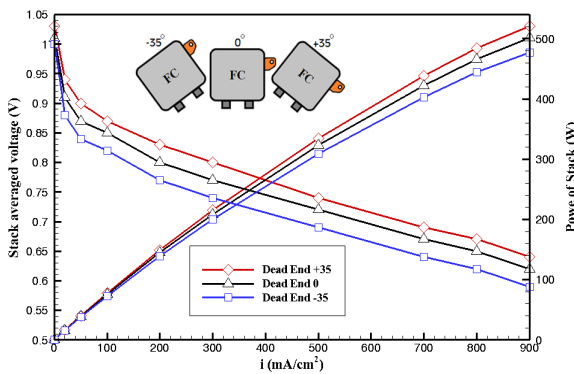


Fig. 9 Polarization curves of the dead-end cascade PEMFC stack under three different orientations.

An automatic control system is applied to open and close the feed lines and to control the purge process.

Since both the anode and cathode sides of the PEM fuel cell are in the dead-end mode, accumulated liquid water is only discharged after purges. As a result, when the valve is closed, the accumulated water blocks part of the active area of PEMFC and causes the stack voltage to drop. However, when the purge valve is open, the voltage increases due to the removal of liquid water from the purged cells of the PEM fuel cell.

Fig. 10 demonstrates three stack voltages measured for three different fuel cell currents. The experimental and simulated outputs are compared in this figure. As can be observed, the stack voltage decreases when its current increases; however, due to the relationship between stack current and the level of water flooding inside the GDL, the voltage drop increases for higher current density as shown in the following figure. Moreover, for a higher stack current, more time is needed to remove the accumulated water completely from the 2nd stage of the PEMFC. The maximum relative error between the numerical results and the experimental data occurs for , and its value is less than 0.8%. In Fig. 10, the purge interval time is considered to be 9.5 s.

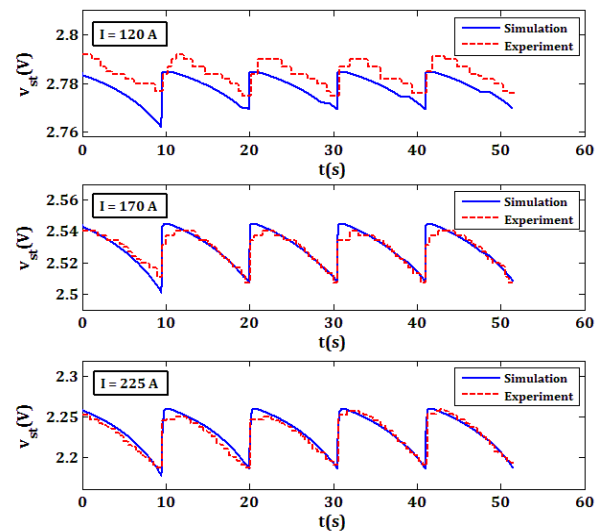


Fig. 10 Voltages of the dead-end cascade-type PEMFC stack for different stack current.

The effective voltage and current density of all three sections (s1: cell 1, s2: cells 2 & 3, and s3: cell 4) of the desired fuel cell stack are shown in Fig. 11 and Fig. 12, respectively. The liquid water produced in the first section of both the anode and the cathode of the PEMFC is continuously discharged by the reactive gases. Therefore, the effective surface area of the membrane in the second part of the stack has not changed, and as a result, the effective voltage and current density of this part of the PEMFC is constant as shown in Fig. 11 and Fig. 12. By increasing the liquid water in the gas diffusion layer, the effective membrane active surface is reduced, which increases the effective current density and decreases the voltage of the stack. Due to the low rate of liquid water production in the anode side channels, the effective current density and voltage variations of the third section of the fuel cell series are almost negligible. However, the amount of water produced in the fuel cell cathode side channels has a significant effect on the effective voltage and current density of the first section of the stack. Fig. 12 shows the effective current density of the various sections of the fuel cell and confirms the above description.

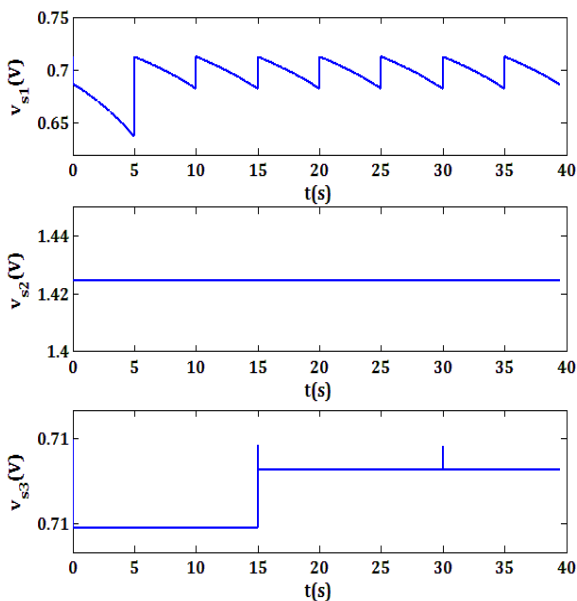


Fig. 11 Voltages of different sections of the dead-end cascade-type PEMFC stack.

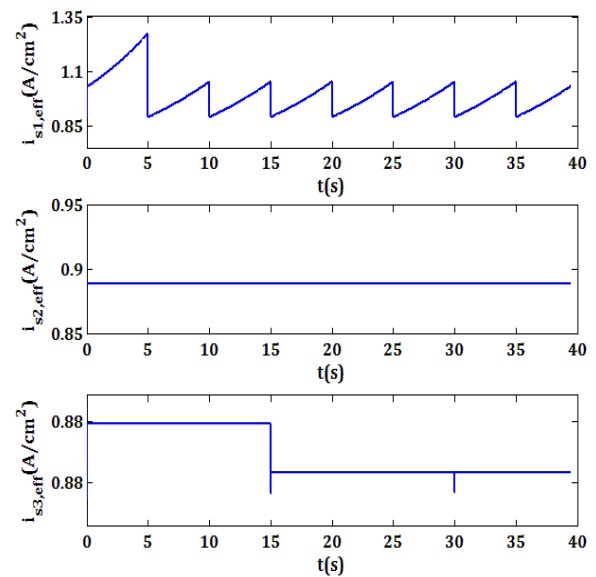


Fig. 12 Effective current density of different sections of the dead-end cascade-type PEMFC stack.

One of the most important issues in the dead-end operation is the fluctuation of stack pressure. High pressure fluctuations damage the MEA and reduce the lifetime of the stack. Conventionally, researchers employ a solenoid valve at the outlet of the stack to purge the accumulated water and impurities. Accordingly, a sudden pressure drop occurs when purging a high volume of reactants in the dead-end mode. It has been proven that using a needle valve before the solenoid valve decreases the fluctuation of pressure in the dead-end mode. In other words, decreasing the reactant pressure before the solenoid valve and increasing the purge duration time leads to a decrease in fluctuations of pressure for the same amount of gas purge. Similar to a cascade type design, the number of operating cells in the dead-end mode decreases, so the fluctuation of pressure is connected with a few cells. The pressure fluctuation of both the anode and cathode sides of the dead-end PEM fuel cell stack is depicted in Fig. 13. As demonstrated, the pressure fluctuation is controlled with the aforementioned method. Moreover, the pressure fluctuation of the cathode side is higher than that of the anode side due to the additional water accumulation.

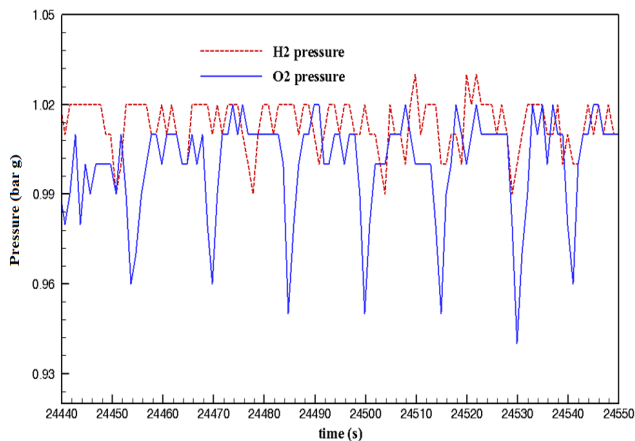


Fig. 13 Pressure fluctuation of the anode and cathode sides of the dead-end PEMFC stack.

The cell voltages for certain values of the purge interval and purge duration time are shown in Fig. 14. As can be seen, the fluctuation of purge cell voltage of the cathode side is higher than that of the anode side. This phenomenon is associated with the accumulation of more liquid water and impurity at the purge cell of the cathode side. The voltage level of the first cell, the oxygen purge cell, is lower than all cell voltages due to the accumulation of water and impurities in the solute. The second and third intermediate cells, which operate in the open end state, have a higher voltage level than the rest of the cells.

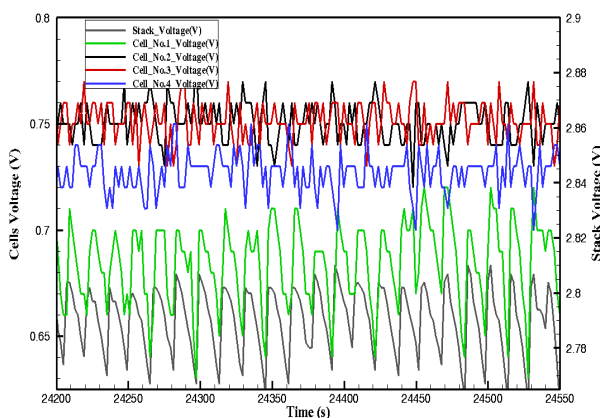


Fig. 14 Voltages of stack and different cells operating in the dead-end mode (purge interval=10 s and purge duration time=2 s).

Fig. 15 displays the cells' voltage fluctuation for different current densities. The results indicate that increasing current density has a significant effect on the

voltage drop of the purge cell of the cathode side. As shown, increasing the current density causes the produced water to increase, which results in an increase in the purge cell voltage drop. Therefore, the purge interval time and the purge duration time should be controlled in accordance with the value of the current density. Moreover, the voltage-based method can be applied to optimize the purging process at high current density.

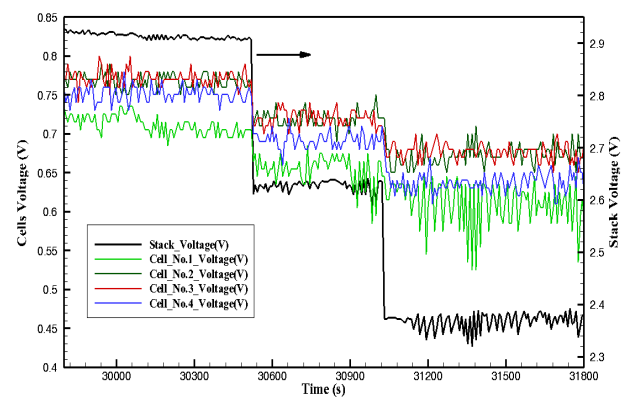


Fig. 15 Effect of current density on voltages of stack and different cells operating in the dead-end mode (purge interval time=10 s and purge duration time=2 s).

Conclusion

In this paper, a 4-cells dead-end cascade-type H_2/O_2 PEM fuel cell was designed, fabricated, and tested. Both the anode and cathode sides of the considered PEMFC stack operated in a dead-end mode. Humidifiers and water separators were integrated with the stack resulting in an increase in volume power density of the PEM fuel cell. In a dead-end mode, the end stage is designed in such a way to entirely use the reactant gases in the operation. Periodical purging was utilized to remove the accumulated water or impurities of the cascade-type PEM fuel cell stack. The results showed that the performance of dead-end and flow-through stacks were almost the same, but the values of reactants stoichiometry for the flow-through PEMFC stack were much greater than the values for the dead-end PEMFC stack. This difference reveals that the complex design of the dead-end PEM fuel cell stack results in a minimum required consumption of reactant gases. Moreover, the voltage fluctuation of

the considered cascade-type PEMFC stack was reduced compared to the conventional dead-end stack. Due to the production of more liquid water at the cathode side, the fluctuation of the purge cell voltage and the pressure fluctuation of the cathode side was higher than those of the anode side. A Mathematical Model developed in this paper was used to accurately predict the performance of a Fuel Cell stack with an integrated humidifier and water separator in the dead-end mode under various operating conditions. Hence, the Mathematic Model can help to optimize the Fuel Cell components design.

Appendix:

Humidifier mathematical model

The terms in Eqs. (1)-(4) are introduced as:

$$\dot{m}_{i,in,Hu(i)} = k_{b,Hu(i)}(p_{b,Hu(i)} - p_{Hu(i)})$$

$$\dot{m}_{i,out,Hu(i)} = \frac{m_{i,Hu(i)}}{m_{i,Hu(i)} + m_{v,Hu(i)}} k_{a,Hu(i)}(p_{Hu(i)} - p_{a,Hu(i)})$$

$$\dot{m}_{v,memb,Hu(i)} = (D_w)_{Hu} \frac{(c_2)_{Hu(i)} - (c_1)_{Hu(i)}}{t_{m,Hu}} M_v A_{Hu(i)}$$

$$\dot{m}_{v,out,Hu(i)} = \frac{m_{v,Hu(i)}}{m_{i,Hu(i)} + m_{v,Hu(i)}} k_{a,Hu(i)}(p_{Hu(i)} - p_{a,Hu(i)})$$

where $i=O_2,H_2$, t_m is the membrane thickness and k is orifice constant. Subscripts “b,Hu(i)” and “a,Hu(i)” denote before -humidifier and after -humidifier, respectively. Moreover, $p_{Hu(i)}$ denotes total pressure in i-humidifier. D_w is the membrane vapor transfer coefficient which can be calculated as:

$$(D_w)_{Hu} = 1.82 \times 10^{-10} e \left[6000 \times \left(\left(\frac{1}{303} \right) - \left(\frac{1}{T_{Hu}} \right) \right) \right]$$

Furthermore, the volumetric concentrations of the membrane matrix in contact with reactants and water, c_1 and c_2 can be obtained as:

$$(c_j)_{Hu(i)} = \left(\frac{\rho_{memb,dry,Hu}}{M_{memb,dry,Hu}} \right) \lambda_{j,Hu(i)} \quad \text{and } j=1,2$$

$\lambda_{j,Hu(i)}$ denotes the water contents j-side chain of the i-humidifier membrane, and can be evaluated by the following equation:

$$\lambda_{j,Hu(i)} = 0.043 + 17.81 \phi_{j,Hu(i)} - 39.85 \phi_{j,Hu(i)}^2 + 36 \phi_{j,Hu(i)}^3 \quad \text{with } i=O_2,H_2 \text{ and } j=1,2$$

Relative humidity of oxygen and hydrogen humidifiers gases can be expressed as:

$$\phi_{j,Hu(i)} = \frac{P_{v,Hu(i)}}{P_{sat}(T_{Hu})}$$

where $P_{v,Hu(i)}$ is partial pressure of water vapor which can be calculated using ideal gas law.

Separator mathematical model

$\dot{m}_{l,an,in,FC(S_3)}$ and $\dot{m}_{l,ca,in,FC(S_1)}$ are assumed to be zero. The subscript “FC(S)”, “an” and “ca” express the section, anode side and cathode side of the fuel cell stack, respectively.

PEM fuel cell stack mathematical model

The terms of Eqs. (5)-(10) can be defined as:

$$\dot{m}_{H_2,in,FC(S_1)} = \dot{m}_{H_2,out,Hu(H_2)} \times \left(\frac{n_{s_i}}{n_{st_1}} \right) \quad \text{with } i=1,2$$

$$\dot{m}_{H_2,in,FC(S_3)} = \dot{m}_{H_2,out,FC(S_1)} + \dot{m}_{H_2,out,FC(S_2)} \quad \text{with } i=1,2$$

$$\dot{m}_{H_2,out,FC(S_1)} = \frac{\dot{m}_{H_2,FC(S_1)}}{\dot{m}_{H_2,FC(S_1)} + \dot{m}_{v,an,FC(S_1)}} k_{a,an,st_1} (P_{an,FC(S_1)} - P_{an,FC(S_3)})$$

$$\dot{m}_{H_2,reacted,FC(S_1)} = M_{H_2} \times \frac{n_{si} I_{st}}{2F} \quad \text{with } i=1,2,3$$

$$\dot{m}_{v,an,in,FC(S_1)} = \dot{m}_{v,out,Hu(H_2)} \times \left(\frac{n_{s_i}}{n_{st_1}} \right) \quad \text{with } i=1,2$$

$$\dot{m}_{v,an,in,FC(S_3)} = \dot{m}_{v,an,out,FC(S_1)} + \dot{m}_{v,an,out,FC(S_2)} \quad \text{with } i=1,2$$

$$\dot{m}_{v,an,out,FC(S_1)} = \frac{\dot{m}_{v,an,FC(S_1)}}{\dot{m}_{H_2,FC(S_1)} + \dot{m}_{v,an,FC(S_1)}} k_{a,an,st_1} (P_{an,FC(S_1)} - P_{an,FC(S_1)})$$

$$\dot{m}_{v,an,GDL2ch,FC(S_1)} = N_{v,an,FC(S_1)} M_v A_{eff,FC(S_1)} n_{S_i} \quad \text{with } i=1,2,3$$

$$\dot{m}_{evap,an,FC(S_i)} = \min \left(A_{eff,FC(S_i)} (p_{sat}(T_{FC}) - p_{v,an,FC(S_i)}) \sqrt{\frac{M_v}{2\pi RT_{FC}}}, \dot{m}_{i,an,GDL2ch,FC(S_i)} \right)$$

with $i=1,2,3$

$$\dot{m}_{i,an,GDL2ch,FC(S_i)} = -A_{eff,FC(S_i)} n_{S_i} \rho_w \frac{KS_{an,FC(S_i)}^3}{\mu_l} \left| \frac{dp_{c,an,FC(S_i)}}{dS_{an,FC(S_i)}} \right| \frac{S_{an,FC(S_i)}}{t_{GDL}}$$

$$\dot{m}_{O_2,in,FC(S_i)} = \dot{m}_{O_2,out,Hu(O_2)} \times \left(\frac{n_{S_i}}{n_{st_1}} \right)$$

with $i=2,3$

$$\dot{m}_{O_2,in,FC(S_1)} = \dot{m}_{O_2,out,FC(S_2)} + \dot{m}_{O_2,out,FC(S_3)}$$

with $i=2,3$

$$\dot{m}_{O_2,out,FC(S_i)} \frac{m_{O_2,FC(S_i)}}{m_{O_2,FC(S_i)} + m_{v,ca,FC(S_i)}} = k_{a,ca,st_1} (p_{ca,FC(S_i)} - p_{ca,FC(S_i)})$$

$$\dot{m}_{O_2,reacted,FC(S_i)} = M_{O_2} \times \frac{n_{S_i} I_{st}}{4F}$$

with $i=1,2,3$

$$\dot{m}_{v,ca,in,FC(S_i)} = \dot{m}_{v,out,Hu(O_2)} \times \left(\frac{n_{S_i}}{n_{st_1}} \right)$$

with $i=2,3$

$$\dot{m}_{v,ca,in,FC(S_i)} = \dot{m}_{v,ca,out,FC(S_2)} + \dot{m}_{v,ca,out,FC(S_3)}$$

with $i=2,3$

$$\dot{m}_{v,ca,out,FC(S_i)} \frac{m_{v,ca,FC(S_i)}}{m_{O_2,FC(S_i)} + m_{v,ca,FC(S_i)}} = k_{a,ca,st_1} (p_{ca,FC(S_i)} - p_{ca,FC(S_i)})$$

$$\dot{m}_{v,ca,GDL2ch,FC(S_i)} = N_{v,ca,FC(S_i)} M_v A_{eff,FC(S_i)} n_{S_i}$$

with $i=1,2,3$

$$\dot{m}_{evap,ca,FC(S_i)} = \min \left(A_{eff,FC(S_i)} (p_{sat}(T_{FC}) - p_{v,ca,FC(S_i)}) \sqrt{\frac{M_v}{2\pi RT_{FC}}}, \dot{m}_{i,ca,GDL2ch,FC(S_i)} \right)$$

with $i=1,2,3$

$$\dot{m}_{i,an,GDL2ch,FC(S_i)} = A_{eff,FC(S_i)} n_{S_i} \rho_w \frac{KS_{ca,FC(S_i)}^3}{\mu_l} \left| \frac{dp_{c,ca,FC(S_i)}}{dS_{ca,FC(S_i)}} \right| \frac{S_{ca,FC(S_i)}}{t_{GDL}}$$

“ n_{S_i} ” and “ n_{st_i} ” denote the number of cells of the section and the stage of fuel cell stack, respectively. Moreover, S is reduced water saturation which can be defined as:

$$S_{j,FC(S_i)} = \begin{cases} \frac{S_{j,FC(S_i)} - S_{im}}{1 - S_{im}} & S_{im} < S_{j,FC(S_i)} \leq 1 \\ 0 & 0 \leq S_{j,FC(S_i)} \leq S_{im} \end{cases}$$

with $i=1,2,3$
and $j=an,ca$

S_{im} is liquid water immobile saturation and $S_{j,FC(S_i)}$ can be obtained as follows:

$$S_{j,FC(S_i)} = \frac{V_{l,j,GDL,FC(S_i)}}{V_p}$$

with $i=1,2,3$
and $j=an,ca$

V_p is volume of gas diffusion layer porosity. The terms $N_{v,an,FC(S_i)}$ and $N_{v,ca,FC(S_i)}$ can be evaluated as follows:

$$N_{v,an,FC(S_i)} = \langle D_{v,an,FC(S_i)} \rangle \frac{c_{v,an,FC(S_i)} - c_{v,an,GDL,FC(S_i)}}{t_{GDL}}$$

with $i=1,2,3$

$$N_{v,ca,FC(S_i)} = -\langle D_{v,ca,FC(S_i)} \rangle \frac{c_{v,ca,FC(S_i)} - c_{v,ca,GDL,FC(S_i)}}{t_{GDL}}$$

with $i=1,2,3$

where:

$$\langle D_{v,ca,FC(S_i)} \rangle = D_v \varepsilon \left(\frac{\varepsilon - 0.11}{1 - 0.11} \right)^{0.785} (1 - S_{j,FC(S_i)})$$

with $i=1,2,3$
and $j=an,ca$

$$c_{v,j,FC(S_i)} = \frac{p_{v,j,FC(S_i)}}{RT_{FC}}$$

with $i=1,2,3$
and $j=an,ca,anGDL,caGDL$

$$R_{evap,j,FC(S_i)} = \gamma \frac{p_{sat}(T_{FC}) - p_{v,j,GDL,FC(S_i)}}{RT_{FC}}$$

with $i=1,2,3$
and $j=an,ca$

$$N_{v,gen,FC(S_i)} = \frac{I_{st}}{2FA_{eff,FC(S_i)}}$$

with $i=1,2,3$

$$N_{v,memb,FC(S_i)} = n_{d,FC(S_i)} \frac{10^4 i_{FC(S_i)}}{F} - (D_w)_{FC(S_i)} \frac{(c_v)_{ca,FC(S_i)} - (c_v)_{an,FC(S_i)}}{t_{m,FC}}$$

$$p_{c,j,FC(S_i)} = \frac{\sigma \cos \theta_c}{(K/\varepsilon)^{0.5}} \left[1.417 S_{j,FC(S_i)} - 2.120 S_{j,FC(S_i)}^2 + 1.263 S_{j,FC(S_i)}^3 \right]$$

with $i=1,2,3$
and $j=an,ca$

$$\dot{m}_{i,out,FC(S_3)} = \begin{cases} \frac{m_{i,FC(S_3)}}{m_{H_2,FC(S_3)} + m_{v,an,FC(S_3)}} k_{a,an,st_2} (p_{an,FC(S_3)} - p_{atm}) & \text{if } R \left(\frac{t}{t_{p,c,an}} \right) \leq t_{p,o,an} \\ 0 & \text{if } R \left(\frac{t}{t_{p,c,an}} \right) > t_{p,o,an} \end{cases}$$

$= H_2, (v, an)$
 $= O_2, (v, ca)$

$$\dot{m}_{i,out,FC(S_1)} = \begin{cases} \frac{m_{i,FC(S_1)}}{m_{O_2,FC(S_1)} + m_{v,ca,FC(S_1)}} k_{a,ca,st_2} (p_{ca,FC(S_1)} - p_{atm}) & \text{if } R \left(\frac{t}{t_{p,c,ca}} \right) \leq t_{p,o,ca} \\ 0 & \text{if } R \left(\frac{t}{t_{p,c,ca}} \right) > t_{p,o,ca} \end{cases}$$

$$\dot{m}_{l,an,out,FC(S_i)} = \begin{cases} k_{l,a,an,st_2} (p_{an,FC(S_i)} - p_{atm}) & \text{if } R \left(\frac{t}{t_{p,an}} \right) \leq t_{p,an} \\ 0 & \text{if } R \left(\frac{t}{t_{p,an}} \right) > t_{p,an} \end{cases}$$

$$\dot{m}_{l,ca,out,FC(S_i)} = \begin{cases} k_{l,a,ca,st_2} (p_{ca,FC(S_i)} - p_{atm}) & \text{if } R \left(\frac{t}{t_{p,ca}} \right) \leq t_{p,ca} \\ 0 & \text{if } R \left(\frac{t}{t_{p,ca}} \right) > t_{p,ca} \end{cases}$$

where R is the remainder after division.

PEM fuel cell electrochemical model

$$E_{Nemst,FC(S_i)} = 1.229 - 8.5 \times 10^{-4} (T_{FC} - 298.15) + 4.308$$

$$\times 10^{-5} T_{FC} \left[\ln \frac{p_{H_2,FC(S_i)}}{101325} + \frac{1}{2} \ln \frac{p_{O_2,FC(S_i)}}{101325} \right]$$

$$V_{act,FC(S_i)} = -(\xi_1 + \xi_2 T_{FC} + \xi_3 T_{FC} \ln(10^4 \times A_{FC} i_{FC(S_i)})) + \xi_4 T_{FC} \ln(C_{O_2,FC(S_i)}^*)$$

$$V_{ohmic,FC(S_i)} = (R_{m,FC(S_i)} + R_c) I_{st}$$

$$V_{conc,FC(S_i)} = -\frac{RT_{FC}}{2F} \ln \left(1 - \frac{i_{FC(S_i)}}{i_{max}} \right)$$

where $i=1,2,3$ and $\xi_1, \xi_2, \xi_3, \xi_4, R_c$ and i_{max} are constants, $R_{m,FC(S_i)}$ is the equivalent membrane resistance to proton conduction and R_c is the equivalent contact resistance to electron conduction. $R_{m,FC(S_i)}$ and $C_{O_2,FC(S_i)}^*$ can be denoted through the following relations:

$$R_{m,FC(S_i)} = \frac{181.6(t_m)_{FC} \left[1 + 0.03 \times i_{FC(S_i)} + 0.062 \times \left(\frac{T_{FC}}{303} \right) \times i_{FC(S_i)}^{2.5} \right]}{A_{eff,FC(S_i)} \left[\psi - 0.634 - 3 \times i_{FC(S_i)} \right] \times \exp \left[4.18 \times \left(\frac{T_{FC} - 303}{T_{FC}} \right) \right]}$$

$$C_{O_2,FC(S_i)}^* = \frac{p_{O_2,FC(S_i)}}{5.08 \times 10^6 \times \exp(-498/T_{FC})}$$

In all terms $i=1,2,3$

$$p_{Hu(j)} = \frac{R_i T_{Hu}}{V_{Hu(j)}} m_{i,Hu(j)} + \frac{R_v T_{Hu}}{V_{Hu(j)}} m_{v,Hu(j)} \quad \text{with } j=O_2, H_2$$

$$p_{a,Hu(O_2)} = \frac{T_{FC}}{(V_{ca,FC(S_i)} + V_{an,FC(S_i)})} \left[R_{O_2} (m_{O_2,FC(S_2)} + m_{O_2,FC(S_3)}) + R_v (m_{v,ca,FC(S_2)} + m_{v,an,FC(S_3)}) \right]$$

$$p_{a,Hu(H_2)} = \frac{T_{FC}}{(V_{an,FC(S_1)} + V_{ca,FC(S_2)})} \left[R_{H_2} (m_{H_2,FC(S_2)} + m_{H_2,FC(S_3)}) + R_v (m_{v,an,FC(S_1)} + m_{v,ca,FC(S_2)}) \right]$$

$$p_{an,FC(S_i)} = \frac{R_{H_2} T_{FC}}{V_{an,FC(S_i)}} m_{H_2,FC(S_i)} + \frac{R_v T_{FC}}{V_{an,FC(S_i)}} m_{v,an,FC(S_i)}$$

$$p_{H_2,FC(S_i)} = \frac{R_{H_2} T_{FC}}{V_{an,FC(S_i)}} m_{H_2,FC(S_i)}$$

$$p_{v,an,FC(S_i)} = \frac{R_v T_{FC}}{V_{an,FC(S_i)}} m_{v,an,FC(S_i)}$$

$$p_{ca,FC(S_i)} = \frac{R_{O_2} T_{FC}}{V_{ca,FC(S_i)}} m_{O_2,FC(S_i)} + \frac{R_v T_{FC}}{V_{ca,FC(S_i)}} m_{v,ca,FC(S_i)}$$

$$p_{O_2,FC(S_i)} = \frac{R_{O_2} T_{FC}}{V_{ca,FC(S_i)}} m_{O_2,FC(S_i)}$$

$$p_{v,ca,FC(S_i)} = \frac{R_v T_{FC}}{V_{ca,FC(S_i)}} m_{v,ca,FC(S_i)}$$

$$(D_w)_{FC(S_i)} = D_{\lambda,FC(S_i)} e^{\left(\frac{2416 \left(\frac{1}{303} - \frac{1}{T_{FC}} \right)} \right)}$$

$$D_{\lambda,FC(S_i)} = \begin{cases} 10^{-10} & , \lambda_{m,FC(S_i)} < 2 \\ 10^{-10} (1 + 2(\lambda_{m,FC(S_i)} - 2)) & , 2 \leq \lambda_{m,FC(S_i)} \leq 3 \\ 10^{-10} (3 - 1.67(\lambda_{m,FC(S_i)} - 3)) & , 3 \leq \lambda_{m,FC(S_i)} \leq 4.5 \\ 1.25 \times 10^{-10} & , \lambda_{m,FC(S_i)} \geq 4.5 \end{cases}$$

$$\lambda_{m,FC(S_i)} = 0.043 + 17.81 \phi_{m,FC(S_i)}^2 - 39.85 \phi_{m,FC(S_i)}^3$$

$$\phi_{m,FC(S_i)} = \frac{\phi_{an,FC(S_i)} + \phi_{ca,FC(S_i)}}{2}$$

$$(c_v)_{ca,FC(S_i)} = \left(\frac{\rho_{memb,dry,FC}}{M_{memb,dry,FC}} \right) \lambda_{ca,FC(S_i)}$$

$$(c_v)_{an,FC(S_i)} = \left(\frac{\rho_{memb,dry,FC}}{M_{memb,dry,FC}} \right) \lambda_{an,FC(S_i)}$$

$$\lambda_{ca,FC(S_i)} = 0.043 + 17.81 \phi_{ca,FC(S_i)}^2 - 39.85 \phi_{ca,FC(S_i)}^3 + 36 \phi_{ca,FC(S_i)}^3$$

$$\lambda_{an,FC(S_i)} = 0.043 + 17.81 \phi_{an,FC(S_i)}^2 - 39.85 \phi_{an,FC(S_i)}^3 + 36 \phi_{an,FC(S_i)}^3$$

$$n_{d,FC(S_i)} = 0.0029 \lambda_{m,FC(S_i)}^2 + 0.05 \lambda_{m,FC(S_i)} - 3.4 \times 10^{-19}$$

References

[1] T. Wilberforce, A. Alaswad, A. Palumbo, M. Dassisi, A. Olabi, Advances in stationary and portable fuel cell applications, International Journal of Hydrogen Energy, 41(37) (2016) 16509-16522.

[2] E. Alizadeh, M. Barzegari, M. Momenifar, M. Ghadimi, S. Saadat, Investigation of contact pressure distribution over the active area of PEM fuel cell stack, International

- Journal of Hydrogen Energy, 41(4) (2016) 3062-3071.
- [3] M.M. Barzegari, M. Dardel, E. Alizadeh, A. Ramiar, Dynamic modeling and validation studies of dead-end cascade H₂/O₂ PEM fuel cell stack with integrated humidifier and separator, *Applied Energy*, 177 (2016) 298-308.
- [4] E. Alizadeh, M. Khorshidian, S. Saadat, S. Rahgoshay, M. Rahimi-Esbo, Experimental Study on a 1000W Dead-End H₂, *Iranian Journal of Hydrogen & Fuel Cell*, 3 (2016) 183-197.
- [5] E. Alizadeh, M. Ghadimi, M. Barzegari, M. Momenifar, S. Saadat, Development of contact pressure distribution of PEM fuel cell's MEA using novel clamping mechanism, *Energy*, 131 (2017) 92-97.
- [6] F. Barbir, *PEM fuel cells: theory and practice*, Academic Press, 2012.
- [7] M. Rahimi-Esbo, A. Ranjbar, A. Ramiar, E. Alizadeh, M. Aghaee, Improving PEM fuel cell performance and effective water removal by using a novel gas flow field, *international journal of hydrogen energy*, 41(4) (2016) 3023-3037.
- [8] E. Alizadeh, S. Rahgoshay, M. Rahimi-Esbo, M. Khorshidian, S. Saadat, A novel cooling flow field design for polymer electrolyte membrane fuel cell stack, *International Journal of Hydrogen Energy*, 41(20) (2016) 8525-8532.
- [9] D. Jenssen, O. Berger, U. Krewer, Improved PEM fuel cell system operation with cascaded stack and ejector-based recirculation, *Applied Energy*, 195 (2017) 324-333.
- [10] M.M. Barzegari, E. Alizadeh, A.H. Pahnabi, Grey-box modeling and model predictive control for cascade-type PEMFC, *Energy*, (2017).
- [11] F. Migliardini, C. Capasso, P. Corbo, Optimization of hydrogen feeding procedure in PEM fuel cell systems for transportation, *International Journal of Hydrogen Energy*, 39(36) (2014) 21746-21752.
- [12] M.M. Barzegari, M. Dardel, E. Alizadeh, A. Ramiar, Reduced-order model of cascade-type PEM fuel cell stack with integrated humidifiers and water separators, *Energy*, 113 (2016) 683-692.
- [13] I.-S. Han, B.-K. Kho, S. Cho, Development of a polymer electrolyte membrane fuel cell stack for an underwater vehicle, *Journal of Power Sources*, 304 (2016) 244-254.
- [14] H. Nishikawa, H. Sasou, R. Kurihara, S. Nakamura, A. Kano, K. Tanaka, T. Aoki, Y. Ogami, High fuel utilization operation of pure hydrogen fuel cells, *International Journal of Hydrogen Energy*, 33(21) (2008) 6262-6269.
- [15] M. Uno, T. Shimada, K. Tanaka, Reactant recirculation system utilizing pressure swing for proton exchange membrane fuel cell, *Journal of Power Sources*, 196(5) (2011) 2558-2566.
- [16] Y. Lee, B. Kim, Y. Kim, An experimental study on water transport through the membrane of a PEFC operating in the dead-end mode, *International journal of hydrogen energy*, 34(18) (2009) 7768-7779.
- [17] Y. Hou, C. Shen, D. Hao, Y. Liu, H. Wang, A dynamic model for hydrogen consumption of fuel cell stacks considering the effects of hydrogen purge operation, *Renewable energy*, 62 (2014) 672-678.
- [18] Y.-S. Chen, C.-W. Yang, J.-Y. Lee, Implementation and evaluation for anode purging of a fuel cell based on nitrogen concentration, *Applied energy*, 113 (2014) 1519-1524.
- [19] B. Belvedere, M. Bianchi, A. Borghetti, A. De Pascale, M. Paolone, R. Vecci, Experimental analysis of a PEM fuel cell performance at variable load with anodic exhaust management optimization, *international journal of hydrogen energy*, 38(1) (2013) 385-393.
- [20] J.-J. Hwang, Effect of hydrogen delivery schemes on fuel cell efficiency, *Journal of Power Sources*, 239 (2013) 54-63.
- [21] M.M. Barzegari, M. Dardel, A. Ramiar, E. Alizadeh, An investigation of temperature effect on performance of dead-end cascade H₂/O₂ PEMFC stack with integrated humidifier and separator, *International Journal of Hydrogen Energy*, 41(4) (2016) 3136-3146.

[22] I.-S. Han, J. Jeong, H.K. Shin, PEM fuel-cell stack design for improved fuel utilization, *International Journal of Hydrogen Energy*, 38(27) (2013) 11996-12006.

[23] N. Bizon, Fuel saving strategy using real-time switching of the fueling regulators in the proton exchange membrane fuel cell system, *Applied Energy*, 252 (2019) 113449.

[24] B. Chen, Z. Tu, S.H. Chan, Performance degradation and recovery characteristics during gas purging in a proton exchange membrane fuel cell with a dead-ended anode, *Applied Thermal Engineering*, 129 (2018) 968-978.

[25] N. Ge, S. Chevalier, D. Muirhead, R. Banerjee, J. Lee, H. Liu, P. Shrestha, K. Fahy, C. Lee, T. Aoki, Detecting cathode corrosion in polymer electrolyte membrane fuel cells in dead-ended anode mode via alternating current impedance, *Journal of Power Sources*, 439 (2019) 227089.

[26] I. Dashti, S. Asghari, M. Goudarzi, Q. Meyer, A. Mehrabani-Zeinabad, D.J. Brett, Optimization of the performance, operation conditions and purge rate for a dead-ended anode proton exchange membrane fuel cell using an analytical model, *Energy*, 179 (2019) 173-185.

[27] M. Steinberger, J. Geiling, R. Oechsner, L. Frey, Anode recirculation and purge strategies for PEM fuel cell operation with diluted hydrogen feed gas, *Applied energy*, 232 (2018) 572-582.

[28] W. Bette, D. Coerlin, H. Stenger, Cascade fuel cell system, in, *Google Patents*, 2009.

[29] C. Siegel, Review of computational heat and mass transfer modeling in polymer-electrolyte-membrane (PEM) fuel cells, *Energy*, 33(9) (2008) 1331-1352.